JOURNAL OF MATERIALS SCIENCE 29 (1994) 1284–1289

Ordering in lead magnesium niobate solid solutions

K. PARK, L. SALAMANCA-RIBA, M. WUTTIG
Department of Materials and Nuclear Engineering, University of Maryland, College Park, MD 20742, USA

D. VIEHLAND
Materials Research Laboratory, and Department of Materials Science and Engineering, University of Illinois, Urbana, IL 61801, USA

Nonstoichiometric ordering of magnesium and niobium cations in undoped and lanthanum-doped lead magnesium niobate solid solutions has been investigated by means of high-resolution transmission electron microscopy and computer image simulation. High-resolution lattice images were obtained using different objective apertures for various microscope imaging conditions. Computer image simulations were performed for a wide range of sample thicknesses, defocusing conditions, local Mg/Nb ratios, and long-range order parameters. The simulated images demonstrated that the lattice images of the ordered region are predominantly dependent on the long-range order parameter. By a comparison of the experimental and simulated images, a range of values of the long-range order parameter $0.2 \leqslant S < 0.8$ was obtained for the ordered regions. It was also shown that the ordered structure has a $(NH_4)_3FeF_6$ structure, which consists of alternating magnesium- and niobium-preferred sublattices along the $\langle 111 \rangle$ directions.

1. Introduction

Lead magnesium niobate and other structurally related cubic perovskites, $Pb(B^{I}_{x}B^{II}_{1-x})O_3$, are relaxor ferroelectrics. These materials are characterized by a relaxation of the dielectric permittivity, and an inability to sustain a macroscopic polarization for temperatures significantly below that of the permittivity maximum, T_{max}. Burns and Dacol [1, 2] have shown that a local polarization exists for temperatures far above T_{max}, indicating that the local symmetry is lower than the global. Viehland *et al.* have recently shown that this broken translational invariance of the polarization results in the development of glass-like characteristics in the dielectric [3], polarization [4], and elastic [5] responses, where there is the development of a frozen state below a characteristic temperature. In general, spin-glass-like behaviour occurs in systems which cannot establish conventional long-range order due to some form of chemical [6–8] or structural [9–11] inhomogeneity. This underlying disorder has yet to be fully elucidated for the relaxor ferroelectric, although it has been believed to be related to the existence of ordered domains [12, 13].

Ordering in $Pb(Mg_{1/3}Nb_{2/3})O_3$ (PMN) has been suggested to arise due to a compositional segregation, resulting in some regions being magnesium-enriched [7, 8]. The scale of the ordered regions was $\sim$ 2–5 nm, which did not coarsen with annealing time. These ordered regions were subsequently hypothesized to have local Mg:Nb ratio of 1:1 relative to the global ratio of 1:2, suggesting that a charge imbalance associated with nonstoichiometric ordering may underlie this microstructure and the resultant relaxor behaviour [12, 13]. Although this type of nonstoichiometry may exist, the Mg:Nb occupancy on the B-sublattices in the ordered structure has yet to be determined. The ordered structures of PMN and $Pb(Sc_{1/2}Ta_{1/2})O_3$ (PST) have previously been investigated using high-resolution transmission electron microscopy (HRTEM) [14–16]. However, quantitative information on the ordered structure of the relaxor ferroelectrics to date was not reported. The purpose of this study is to elucidate quantitatively the microstructure of PMN by means of high-resolution lattice imaging and computer image simulation. The influence of long-range order parameter on the lattice images of the ordered regions is also described in this work.

2. Experimental procedure

The samples used in this study were undoped and lanthanum-doped PMN solid solutions. These samples were prepared by the precalcination method [17]; MgO and Nb_2O_5 were prereacted to form columbite, and then milled with the appropriate proportions of PbO and La_2O_3. Lanthanum additions were used to enlarge the size of the ordered domains, increasing the available information concerning the atomic arrangement of the ordered structure.

The samples for HRTEM were prepared by mechanical grinding, dimple grinding, and subsequent ion-milling at liquid nitrogen temperature. The ion-milling was done using 4.5 keV Ar^+ ions and 1 mA

0022–2461

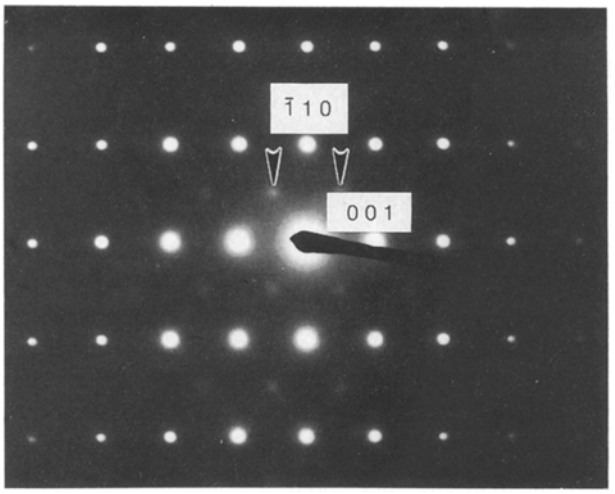

Figure 1 (110) electron diffraction pattern from undoped PMN. Two superlattice reflections (F-spots) are marked by arrowheads.

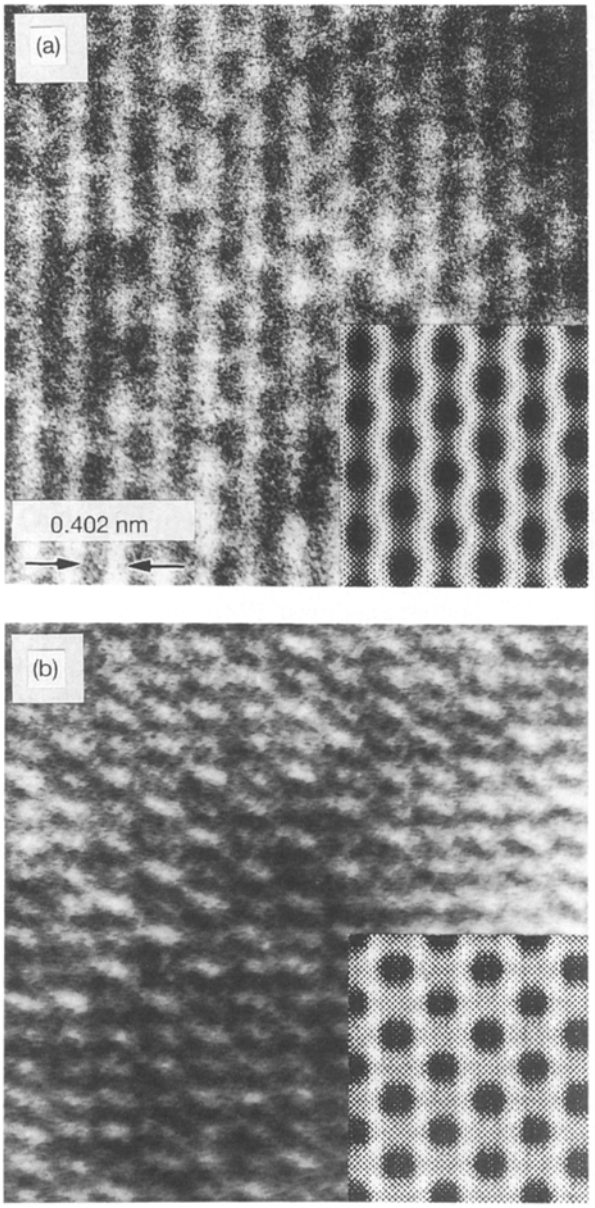

Figure 2 Experimental (110) lattice images of an ordered region for 5% lanthanum-doped PMN for two different defocusing values. The insets show simulated images for a sample thickness of 12.5 nm, Mg : Nb = 1 : 2, long-range order parameter of 0.6, and defocusing values of (a) − 64 nm and (b) − 76 nm. An objective aperture with radius of 3.37 nm^{-1} was used to obtain these images.

current in order to minimize ion-induced damage. The structural studies were performed using a Jeol 2000FX-II transmission electron microscope (TEM) which was operated at an accelerating voltage of 200 keV. The microscope has spherical and chromatic aberration coefficients of 2.3 and 2.2 mm, respectively, with resolutions of 0.28 nm (point) and 0.14 nm (lattice). The Scherzer focus of the TEM is − 76 nm. Experimental lattice images of the ordered structure were obtained using different objective apertures for various defocusing conditions. Simulated lattice images using the multislice method [18–20] with allowance for factors such as specific composition and occupancy of the cations on the B-site sublattice, sample thickness, and microscope imaging conditions were obtained, and the results were compared with the experimentally obtained lattice images.

3. Electron diffraction patterns

Fig. 1 shows a (1 1 0) electron diffraction pattern from undoped PMN. In addition to (strong) allowed reflections originating from the cubic perovskite structure, extra (weak) superlattice reflections (F-spots), marked by arrowheads, appear at positions $(h + \frac{1}{2}, k + \frac{1}{2}, l + \frac{1}{2})$ with respect to the fundamental reflections of the primitive perovskite unit cell ($a_o \approx 0.402$ nm). The existence of these superlattice reflections clearly confirms that some regions of the sample correspond to an ordered structure which gives rise to doubling ($2a_0 \times 2a_0 \times 2a_0$) of the primitive perovskite unit cell, as previously reported [7, 8]. The intensity of the superlattice reflections increases as the contents of the dopant La^{3+} in PMN increase, thereby indicating an increase in the size of ordered domains and/or the degree of order. These results are consistent with those presented for lanthanum-doped PMN by Chen *et al.* [12] and Lin and Wu [21]. Dark-field images obtained using the $\frac{1}{2}(1\,\bar{1}\,1)$ spot shown in Fig. 1 revealed

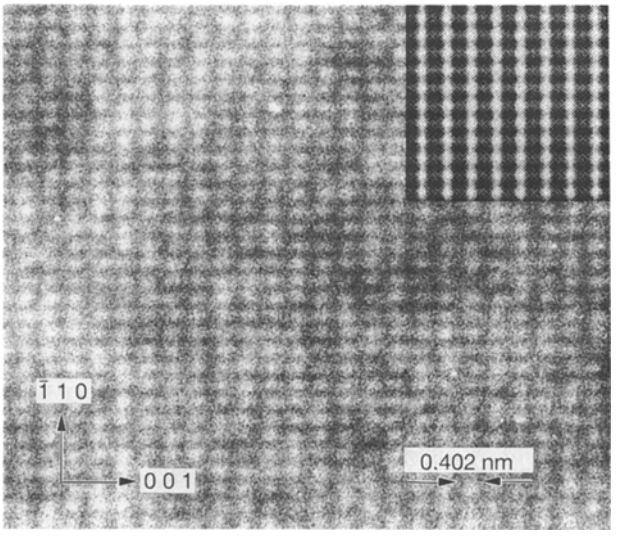

Figure 3 Experimental (110) lattice image showing a disordered region for 5% lanthanum-doped PMN. The inset shows a simulated image for a sample thickness of 12.5 nm, defocus of − 76 nm, and long-range order parameter 0.0. An objective aperture with radius of 3.37 nm^{-1} was used to obtain these images.

that the size of the ordered regions was in the range 4–20 nm.

4. High-resolution lattice images

In order to investigate the microstructure of the ordered and disordered regions for undoped and lanthanum-doped PMN at the atomic level, several high-resolution lattice images in the [1 1 0] projection were obtained experimentally using different objective apertures for various microscope imaging conditions. Some examples are shown in Figs 2–4. Ordered regions with relatively large diameters $\sim$ 10–20 nm and from thin areas ($\leqslant$ 20 nm) of the samples were selected for the analyses. This selection increased the probability of the electron beam to traverse only that region and not a superposition of ordered and disordered regions. Experimental (1 1 0) lattice images from the same area of an ordered region but for two different defocusing values for 5% lanthanum-doped PMN are shown in Fig. 2a and b. These lattice images were obtained using an aperture of radius of 3.37 nm^{-1}, which allowed for contributions from the $\pm(0\,0\,1)$, $\pm(1\,\bar{1}\,0)$, $\pm\frac{1}{2}(\bar{1}\,1\,1)$ and $\pm\frac{1}{2}(1\,\bar{1}\,1)$ reflections. In these figures, a contrast modulation along the $\langle 1\,1\,1\rangle$ directions, and the (0 0 1) and (1 $\bar{1}$ 0) lattice fringes with a pseudo-hexagonal pattern are clearly observed. The wavelength of the contrast modulation is $\sim$ 0.407 nm, as obtained from optical diffractograms taken from the negatives of the lattice images. This value approximately corresponds to twice the calculated (1 1 1) interplanar spacing, strongly implying that the ordered structure corresponds to a doubling of the perovskite unit cell which arises from the formation of two distinct B-site cation sublattices [7, 8].

In contrast, the lattice images of disordered regions for 5% lanthanum-doped PMN taken with approximately the same conditions showed tetragonal patterns, as shown in Fig. 3. This lattice image was obtained using an aperture of radius of 3.37 nm^{-1} and a defocusing value close to the Scherzer value. The same tetragonal pattern was observed from disordered regions, regardless of the objective aperture size, sample thickness, and defocusing value. It is important to note that the boundaries between ordered and disordered regions were coherent, suggesting that there is no appreciable change in the lattice constant between these regions other than a doubling of the perovskite unit cell.

Other regions of the samples showed lattice images with patterns between those shown in Figs 2 and 3. One example of these is shown in Fig. 4 in which (1 1 0) lattice images from the same area of an ordered region of a 5% lanthanum-doped PMN for two different defocusing values of the objective lens, using a large aperture of radius of 6.05 nm^{-1} can be seen. This

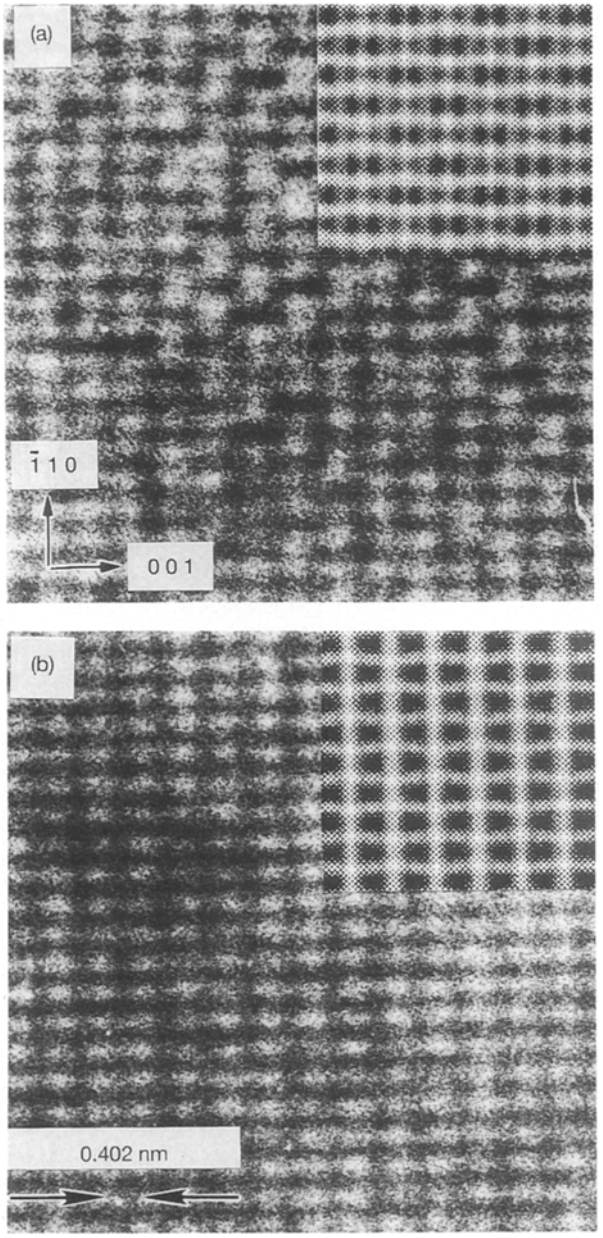

Figure 4 Experimental (110) lattice images of an ordered region for 5% lanthanum-doped PMN for two different defocusing values. The insets show simulated images for a sample thickness of 12.5 nm, Mg:Nb = 1:2, long-range order parameter of 0.2, and defocusing values of (a) – 88 nm and (b) – 100 nm. An objective aperture with radius of 6.05 $nm^{-1}$was used to obtain these images.

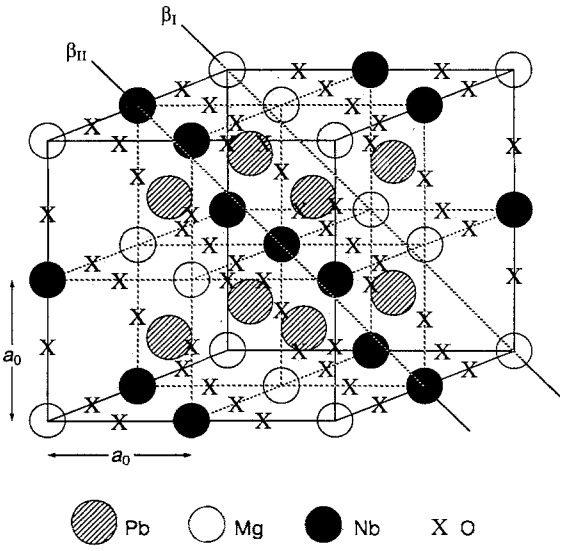

Figure 5 Proposed model for the atomic configuration of ordered PMN [22], illustrating the formation of two distinct B-site cation sublattices, β_I and β_{II}, for magnesium and niobium, respectively.

aperture allows for contributions from additional reflections including: $\pm\frac{1}{2}(1\,\bar{1}\,3)$, $\pm\frac{1}{2}(\bar{1}\,1\,3)$, $\pm(3\,\bar{3}\,1)$, $\pm(\bar{3}\,3\,1)$, $\pm(0\,0\,2)$, $\pm(\bar{1}\,1\,1)$ and $\pm(1\,\bar{1}\,1)$ reflections. Contrast fluctuations, indicative of the ordered structure are observed in Fig. 4a, while essentially no contrast fluctuations are observed in Fig. 4b, even though both images correspond to the same sample area. The lattice image shown in Fig. 4b more closely resembles those of the disordered regions (see Fig. 3). It should therefore, be noted that lattice imaging in this system is strongly dependent on the experimental conditions, including sample thicknesses and defocusing values. Also, from Figs 2 and 4 it is clear that these images correspond to ordered regions with different long-range order parameter, i.e. different occupancy of magnesium and niobium cations on the B-site sublattices. It is also possible that the difference in long-range order parameter is associated with a difference in the local composition of magnesium and niobium cations within the ordered regions. In order to obtain more insight into the local composition and long-range order parameter of the order region, matching of the experimental and simulated images was carried out by visual comparison of a series of simulated

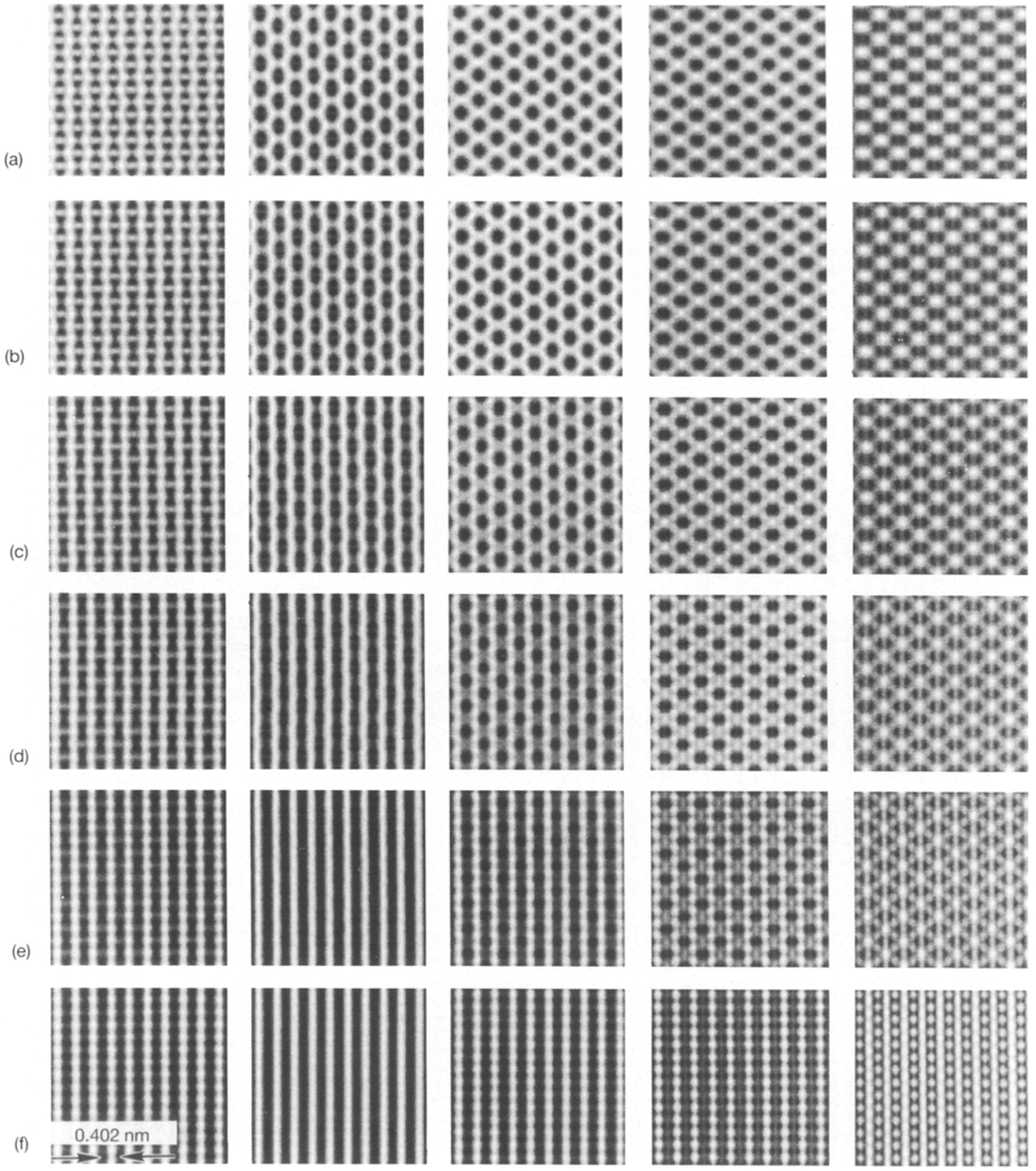

Figure 6 Simulated (110) lattice images from a local Mg:Nb ratio of 1:1 and sample thickness of 12.5 nm for long-range order parameter S = (a) 1.0, (b) 0.8, (c) 0.6, (d) 0.4, (e) 0.2 and (f) 0.0. The defocusing values for each column are, from left to right, $\Delta f = -52, -64, -76, -88$ and -100 nm.

images, obtained for thicknesses ranging from 2.2–20.5 nm in steps of 1.1 nm. For each thickness five different defocusing values were used to calculate the simulated images. Also, the long-range order parameter was varied from 0 to S_{max}, the maximum value. These results are presented in more detail below.

5. Computer-simulated lattice images

Computer image simulations were performed using the multislice method to obtain more detailed information on the ordered structure, and assuming the ordered $(NH_4)_3FeF_6$ structure shown in Fig. 5. In this figure, two crystallographic B-site sublattices are marked, β_I (magnesium preferred-sites) and β_{II} (niobium preferred-sites), corresponding to a 1:1 ordering of alternating magnesium and niobium layers along the $\langle 1\,1\,1 \rangle$ directions. Simulations were carried out for several sample thicknesses, long-range order parameters, S, defocusing values of the objective lens, Δf, and local Mg:Nb ratios (1:1 and 1:2). The sample thicknesses ranged from 2.2–20.5 nm in steps of 1.1 nm, the long-range order parameters ranged from maximum order parameter S_{max} to 0.0, and the defocusing values ranged from − 46 to − 96 nm in steps of 12 nm. The input operating parameters used in these calculations were the voltage (200 kV), the objective aperture radius (3.37 or 6.05 nm^{-1}), the spherical aberration coefficient (2.3 mm), the semi-angle of illumination (1.0 mrad), the half-width of Gaussian spread of vibration (0.0 nm), and the half-width of Gaussian spread of defocus (5 nm).

Figs 6 and 7 show the dependence of simulated images on the long-range order parameter and defocusing value at a sample thickness of 12.5 nm for local Mg:Nb ratios of 1:1 and 1:2, respectively, which were obtained using an aperture of radius of 3.37 nm^{-1}. Complete long-range order ($S = 1.0$) corresponds to all β_I and β_{II} sites being occupied by magnesium and niobium, respectively, and can only be achieved for a local Mg:Nb ratio of 1:1. S_{max} for a local Mg:Nb ratio of 1:2 equals 0.67. The simulated images presented in Figs 6 and 7 show how the long-range order parameter affects the image detail. It is

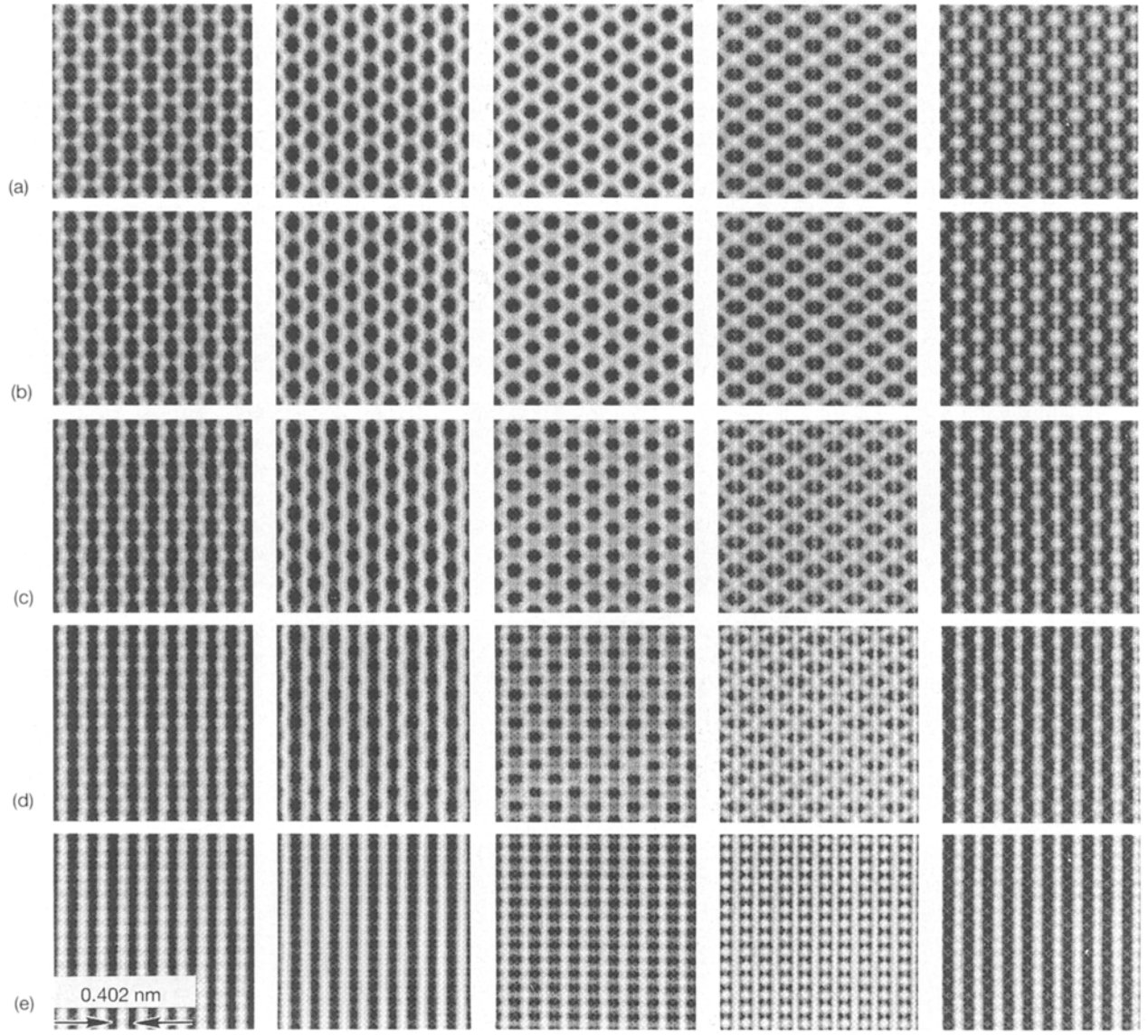

Figure 7 Simulated (110) lattice images from a local Mg:Nb ratio of 1:2 and sample thickness of 12.5 nm for long-range order parameter S = (a) 0.67, (b) 0.6, (c) 0.4, (d) 0.2 and (e) 0.0. The defocusing values for each column are, from left to right, Δf = − 52, − 64, − 76, − 88 and − 100 nm.

evident in these figures that the simulated images slowly change from pseudo-hexagonal to rectangular pattern with decreasing S, thus showing the difference between the ordered and disordered structures at the atomic level. It was also observed that for the same value of S the simulated images obtained for a certain thickness and defocusing value were similar for both Mg:Nb ratios. For example, the lattice images with Mg:Nb = 1:1 and $S = 0.6$ (see Fig. 6c) are nearly identical to those with Mg:Nb = 1:2 and S = 0.6 (see Fig. 7b). Thus, these results clearly demonstrate that the lattice images of ordered regions are strongly sensitive to the value of long-range order parameter, but insensitive to the relative Mg:Nb ratio.

The long-range order parameter of the ordered structure can be estimated by comparing the simulated images with the experimental images. It is extremely difficult to identify the exact value of the long-range order parameter of the ordered structure, because the experimental images are noisy and are not uniform from one area to another. A careful comparison between the experimental and simulated images shown in Figs 2 and 4 indicated that the best match corresponds to $S \approx 0.6$ and $S \approx 0.2$, respectively. The corresponding simulated images are shown as insets to these figures. The comparison was carried out by obtaining a through-focal series of lattice images from the same area and comparing them to similar series of simulated images obtained for different values of the long-range order parameters. The criteria for matching was that all experimental and simulated images in the through-focal series needed to match. The same comparison was carried out from several samples and for two different objective apertures. The result of this investigation indicates that the value of the long-range order parameter varies between 0.6 and 0.2 from one region to another. Furthermore, from this investigation it can be concluded that nonstoichiometric ordering of magnesium and niobium cations along the $\langle 1\,1\,1 \rangle$ directions takes place, i.e. it is not necessary that the local Mg:Nb ratio varies from 1:1 to 1:2 between the ordered and disordered regions. In addition, the results of this comparison also show that the proposed model with a $(NH_4)_3FeF_6$ structure for PMN is valid for the ordered structure.

6. Conclusion

We have observed nonstoichiometric ordering of magnesium and niobium cations in undoped and lanthanium-doped lead magnesium niobate solid solutions along the $\langle 1\,1\,1 \rangle$ directions, giving rise to the doubling of the primitive perovskite unit cell. Simulated images revealed that the lattice images of the ordered regions are dominated by the long-range order parameter. By extensive visual comparison of experimental and simulated images, it was also determined that the value of the order parameter in the ordered regions with a $(NH_4)_3FeF_6$ structure is $0.2 \leqslant S < 0.8$.

Acknowledgements

K. Park and L. Salamanca-Riba thank the National Science Foundation for support under Contract DMR-90-20304, and D. Viehland acknowledges support from the Office of Naval Research.

References

1. G. BURNS and F. H. DACOL, *Sol. State Commun.* **48** (1983) 853.
2. *Idem, ibid.* **58** (1986) 567.
3. D. VIEHLAND, S. JANG, L. E. CROSS, and M. WUTTIG, *Phil. Mag.* **B64** (1991) 335.
4. D. VIEHLAND, J. F. LI, S. J. JANG, L. E. CROSS, and M. WUTTIG, *Phys. Rev.* **B43** (1991) 8316.
5. D. VIEHLAND, S. J. JANG, L. E. CROSS, and M. WUTTIG, *Phil. Mag.* **A64** (1991) 835.
6. U. ATZMONY, E. GUREWITZ, M. MELAMUO, H. PINTO, H. SHAKO, G. GORODESFKY, E. HERMAN, R. HORNREICH, S. SHTRIKMAN and B. WANKLYN, *Phys. Rev. Lett.* **43** (1979) 782.
7. U. KÖBLER and K. BINDER, *J. Magn. Magn. Mater.* **15-18** (1980) 313.
8. D. HÜSER, L. E. WENGER, A. J. VAN DUYNEVELDT and J. A. MYDOSH, *Phys. Rev.* **B27** (1983) 3100.
9. K. KNORR, U. G. VOLKMANN and A. LOIDL, *Phys. Rev. Lett.* **57** (1986) 2544.
10. A. LOIDL, R. FEILE, K. KNORR and J. K. KJEMS, *Physical Review* **B29** (1984) 6052.
11. M. B. SALAMON, K. V. RAO and Y. YESHURUN, *J. Appl. Phys.* **52** (1981) 1687.
12. J. CHEN, H. M. CHAN and M. P. HARMER, *J. Am. Ceram. Soc.* **72** (1989) 593.
13. C. A. RANDALL and A. S. BHALLA, *Jpn J. Appl. Phys.* **29** (1990) 327.
14. H. B. KRAUSE, J. M. COWLEY and J. WHEATLEY, *Acta Crystallogr.* **A35** (1979) 1015.
15. E. HUSSON, M. CHUBB and A. MORELL, *Mater. Res. Bull.* **23** (1988) 357.
16. Z. C. KANG, C. CARANONI, I. SINY, G. NIHOUL and C. BOULESTEIX, *J. Solid State Chem.* **87** (1990) 308.
17. S. L. SWARTZ and T. R. SHROUT, *Mater. Res. Bull.* **17** (1982) 1245.
18. J. M. COWLEY and A. F. MOODIE, *Acta Crystallogr.* **10** (1957) 609.
19. *Idem, ibid.* **12** (1959) 353.
20. *Idem, ibid.* **12** (1959) 360.
21. L. J. LIN and T. B. WU, *J. Am. Ceram. Soc.* **73** (1990) 1253.
22. F. S. GALASSO, in "Structure, Properties and Preparation of Perovskite-Type Compounds", edited by R. Sinoluchowski and N. Kurti (Pergamon Press, New York, 1969) p. 12.

Received 19 October 1992
and accepted 28 July 1993